Front propagation of spatiotemporal chaos

J. W. Kim,[1] J. Y. Vaishnav,[1] E. Ott,[1] S. C. Venkataramani,[2] and W. Losert[1]
[1]*Department of Physics, University of Maryland, College Park, Maryland 20742*
[2]*Department of Mathematics, University of Chicago, Chicago, Illinois 60637*
(Received 6 February 2001; published 20 June 2001)

We study the dynamics of the front separating a spatiotemporally chaotic region from a stable steady region using a simple model applicable to periodically forced systems. In particular, we investigate both the coarsening of the front induced by the inherent ''noise'' of the chaotic region, and the long wavelength dynamics causing the front to develop cusps.

DOI: 10.1103/PhysRevE.64.016215 PACS number(s): 05.45.−a, 46.15.−x, 81.10.Aj

I. INTRODUCTION

In this paper we study the dynamics of the front separating a spatiotemporally chaotic state from a stable steady ordered state. Such situations occur in many experimental settings. In an experiment on a vertically vibrating granular monolayer of spheres [1] both a state at rest on the plate and a chaotically bouncing state are stable. When a small perturbation is applied to the stationary state, the chaotic state is observed to invade the stable state through a propagating front. In a Rayleigh-Bénard convection experiment [2] both straight rolls and spiral defect chaos are stable under some conditions and it is observed that a region of straight rolls is invaded by a region of spiral defect turbulence.

For our study we employ a type of model called a continuum coupled map (CCM) introduced in Ref. [3]. Models of this type (Sec. II) are appropriate to periodically forced systems (such as that in the experiment of Ref. [1]). In common with other generic models, like the complex Ginzburg-Landau equation or the Swift-Hohenberg equation, CCM models are meant to incorporate the minimal basic properties capable of reproducing the phenomena of interest. With this in mind we construct our CCM model to incorporate the essential feature that both a stable steady homogeneous attractor and a spatiotemporally chaotic attractor exist. Using our CCM model, we numerically investigate two phenomena: (i) the coarsening of the front due to the inherent ''noise'' associated with the spatiotemporal chaos (Sec. III), and (ii) cusp formation induced by initial long wavelength perturbations of the front location from the flat state (Sec. IV).

With respect to (i), an important concept used to study various coarsening processes is scaling. For a large number of systems (e.g., see Ref. [4]), it is found that the interface width due to roughening, $w(t)$, increases as a power of time, $w(t)\sim t^{\beta}$. The width eventually saturates at a value that increases as a power of the system size, $w(L_x)\sim L_x^{\alpha}$. These scaling properties are also observed in our model, and we determine and discuss the scaling exponents α and β that we find.

With respect to (ii), we argue that on a long scale [i.e., long compared to $w(t)$], our fronts propagate at constant speed in a direction locally normal to the interface. We show that this basic property explains the mechanism of cusp formation and the evolution of the shape of the fronts observed in our numerical simulations.

II. MODEL

As in Ref. [3], we consider a CCM model that maps a field $\xi_n(\vec{x})$ forward from time n to time $n+1$. With reference to a system driven periodically in time (e.g., as in [1]), we may think of $\xi_n(\vec{x})$, with $n=1,2,\ldots$, as being the system state stroboscopically sampled once each period. Furthermore, we consider $\vec{x}=(x,y)$ to be two dimensional and, for simplicity, we take ξ_n to be a scalar field. The CCM model mapping ξ_n to ξ_{n+1} consists of two steps: The first step is a nonlinear local operation in which a one-dimensional map M is applied to $\xi_n(\vec{x})$ at each point in space,

$$\xi_n'(\vec{x})=M(\xi_n(\vec{x})). \tag{1}$$

The second step is a translationally invariant linear operation coupling the dynamics at nearby spatial locations. The most general such coupling is conveniently expressed in terms of the spatial Fourier transform. If $\hat{\xi}_n(\vec{k})$ is the spatial Fourier transform of $\xi_n(\vec{x})$, then we write $\hat{\xi}_{n+1}(\vec{k})$ as

$$\hat{\xi}_{n+1}(\vec{k})=\check{f}(\vec{k})\hat{\xi}_n'(\vec{k}), \tag{2}$$

from which $\xi_{n+1}(\vec{x})$ is obtained by inverse Fourier transforming.

The model is then specified by the choice of the nonlinear map M and the linear spatial coupling $\check{f}(\vec{k})$. We make these choices so as to include the minimum properties that we hypothesize are relevant for the investigated phenomena [5]. Since we desire the simultaneous existence of a stable steady state as well as a spatiotemporally chaotic state, we choose the map M to have a stable fixed point attractor and a chaotic attractor. A convenient choice having this property is given by

$$M(\xi)=r\xi+A\exp[-(\xi-1)^2/\sigma^2]-A\exp(-1/\sigma^2). \tag{3}$$

Referring to Fig. 1 we see that this map has a stable fixed point at $\xi=0$ for $r<1$. Moreover, any initial point in $\xi<u$ is attracted to this point. We also see from Fig. 1 that the interval $u<\xi<v$ is mapped into itself. Thus there is (at least)

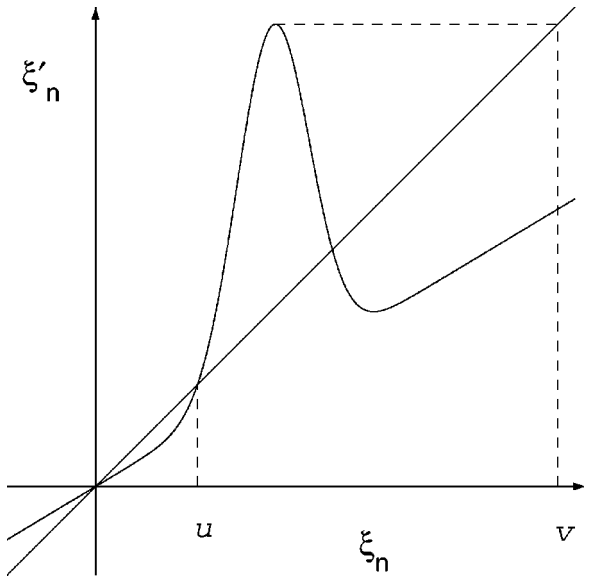

FIG. 1. Schematic (not to scale) of the model map.

one attractor in this interval. For the parameter values A,r, and w that we investigate ($A=7.0,r=0.4,\sigma=0.29$) there is one attractor in $u<\xi<v$ and it is chaotic.

Our choice of the spatial coupling $\check{f}(\vec{k})$ is similarly motivated by a desire for simplicity. We assume that the coupling is isotropic. Thus we can write $\check{f}$ as $\check{f}(\vec{k})=f(k)$, where $k=|\vec{k}|$. Taking $f(k)\geqslant 0$ we write

$$f(k)=\exp[\gamma(k)], \tag{4}$$

where $\gamma(k)$ is a wave-number-dependent growth and/or damping rate per period. Since we want the spatiotemporal chaos to have a finite spatial correlation scale, such a scale must be reflected in our choice of $\gamma(k)$. Denoting this scale by k_0^{-1}, we make the following simple choice [3] for $\gamma(k)$:

$$\gamma(k)=\frac{1}{2}\left(\frac{k}{k_0}\right)^2\left[1-\frac{1}{2}\left(\frac{k}{k_0}\right)^2\right]. \tag{5}$$

Thus $\gamma(k)>0$ (growth) for $k<k_0$, $\gamma(k)$ has its maximum value at $k=k_0$, and $\gamma(k)$ becomes strongly negative (damping) as k becomes large.

Our numerical implementation of this CCM model employs doubly periodic boundary conditions with periodicity lengths L_x in x and L_y in y. The nonlinear map operator is applied at points on a square grid, while the spatial coupling operator (2) employs fast Fourier transforming from $\vec{x}$ to $\vec{k}$ and back.

That $\xi(\vec{x})=0$ is an attractor can be seen by introducing an initial perturbation at wave number $\vec{k}$, $\delta\xi_0\exp(i\vec{k}\cdot\vec{x})$. Linearization of the CCM model about $\xi_0(\vec{x})=0$ then shows that this perturbation evolves with time to $\delta\xi_n\exp(i\vec{k}\cdot\vec{x})$, where $\delta\xi_n=\delta\xi_0[M'(0)f(k)]^n, M'(\xi)\equiv\partial M/\partial\xi$. For the parameters we choose $M'(0)f(k)<1$ for all k [in particular $M'(0)f(k_0)<1$]. Thus the homogeneous state $\xi(\vec{x})=0$ is an attractor for the system. We also find that, as we had anticipated, for other initial conditions there is another attractor which is spatiotemporally chaotic.

Figure 2 shows the properties of the spatiotemporal chaos produced by our model. Figure 2(a) shows the spatial pattern $\xi_n(\vec{x})$ at a representative time. This picture applies to a time $n=45$ evolved from an initial condition where $\xi_0(\vec{x})$ was chosen randomly with uniform distribution between $\xi_0=0$ and $\xi_0=7.5$. Visually, we observe that the pattern appears to have a characteristic scale of the order of k_0^{-1}. This is confirmed by the wave number power spectrum, Fig. 2(b). We note that the only length scales in our model are k_0^{-1}, the system size $L\sim L_x\sim L_y$, and the grid size δ, and that, by our choice $L\gg k_0^{-1}\gg\delta$, we had sought to obtain spatiotemporal chaos with properties independent of L and δ. Figure 2(b), which evidences variation on the scale k_0, conforms with this expectation. Further discussion of the form observed for $|\hat{\xi}(k)|^2$ is given in the Appendix. To characterize the temporal variation of the patterns, Fig. 2(c) shows a plot of the time correlation function $C(\tau)$ defined as

$$C(\tau)=\frac{1}{N_xN_y}\sum_{i,j}^{N_xN_y}C_{i,j}(\tau), \tag{6}$$

$$C_{i,j}(\tau)=\frac{\langle(\xi_{i,j}(t+\tau)-\overline{\xi_{i,j}})(\xi_{i,j}(t)-\overline{\xi_{i,j}})\rangle}{\langle\xi_{i,j}^2(t)-\overline{\xi_{i,j}^2}\rangle}, \tag{7}$$

where $\langle\ldots\rangle$ means time average, $\overline{\xi}=\langle\xi\rangle, N_{x,y}=L_{x,y}/\delta$, and (i,j) denotes the (x,y) location of a grid point. As can be seen from Fig. 2(c) the time correlation function decays to zero with increasing time τ (where τ is an integer), confirming that the temporal behavior is chaotic. We have also examined other parameter values for which (1)–(5) yields spatiotemporal chaos, and we find behavior similar to that in Figs. 2.

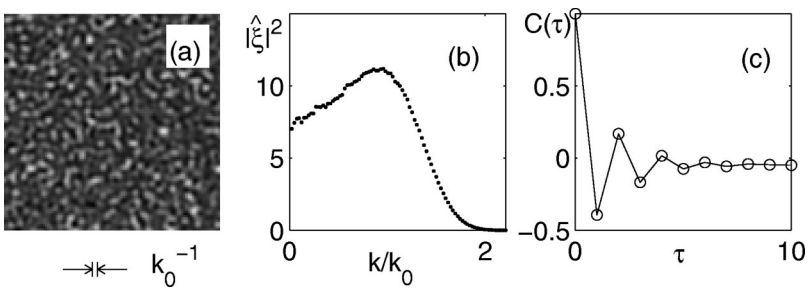

FIG. 2. Spatiotemporal chaos of the CCM model for $A=7.0$, $r=0.4$, and $w=0.29$. (a) A snapshot of $\xi_n(\vec{x})$. Bright regions indicate large amplitude. (b) Wave number power spectrum, averaged over 100 frames. $\hat{\xi}(\vec{k})$ is the Fourier transformation of $\xi(\vec{x})$. (c) Time correlation function $C(\tau)$, Eq. (7).

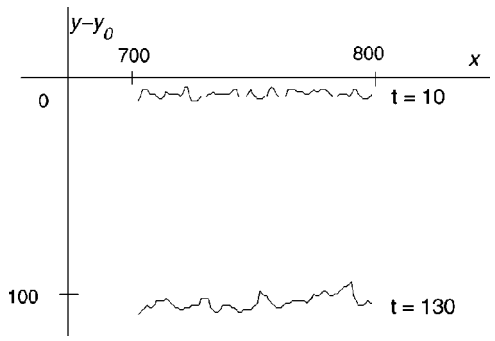

FIG. 3. Coarsening of a flat front. $L_x=1024$.

III. PROPAGATION OF A FLAT FRONT

The main objective of our investigation is to characterize the dynamics of the interface between a spatiotemporally chaotic state and a stable steady state. In our first set of simulations we focus on an initially flat interface, $y=y_0$ at $t=0$. After we generate an initial spatiotemporally chaotic state [Fig. 2(a)], we create the interface by setting the amplitude ξ of all grid points with $y<y_0$ to the stable steady state value $\xi=0$. During further iterations, the front between the chaotic and steady state moves downward, i.e., the chaotic state propagates into the stable steady state, and the front coarsens (see Fig. 3). In order to examine the front dynamics for long times and save computational time, we use a shifting method: On every iterate, we reset ξ to zero in the region adjacent to the bottom ($y=0$) of the periodic box, and, when the front comes close to $y=0$, we shift the whole system upward in the y direction. Due to the periodic boundary conditions, after this shift there will be a region below the front and above $y=0$ that is in the spatiotemporally chaotic regime, and we then set $\xi=0$ in this region.

After an initial transient, the scaling properties of the front are studied using the following definition of the interface width. First, we calculate the average value of ξ at fixed y, $\tilde{\xi}(y)=\int_0^{L_x}\xi(x,y)dx/L_x$. We then note that the basin boundary between the two attractors of the one-dimensional map M is at the unstable fixed point, $u=0.4824$ (Fig. 1), and that the average ξ for the spatiotemporally chaotic state [Fig. 2(a)] is approximately four times the critical value. Thus, we define a lower boundary of the front, y_1, by $\tilde{\xi}(y_1)=u$ and an upper boundary of the front, y_2, by $\tilde{\xi}(y_2)=3u$. The width of the front is then defined as (y_2-y_1).

Because of the inherent ''noise'' generated in the spatiotemporally chaotic region, the proper quantity to study is the ensemble averaged mean of the front widths. We calculate ensembles using many different random initial conditions. Our results for the ensemble averaged width w of the front are obtained by averaging (y_2-y_1) over ten runs for the largest system $L_x=1024$ and over 500 runs for the smallest $L_x=64$. The typical coarsening of the front is shown in Fig. 3.

One observation from our simulations is that the propagation velocity of fronts is constant, except for a few transient initial iterations. That is, the velocity does not depend on time or system size. A constant propagation front velocity is also observed in the experiments in Refs. [1] and [2]. To minimize the effect of the initial transient, we redefine time as the total increase in the area of the chaotic state.

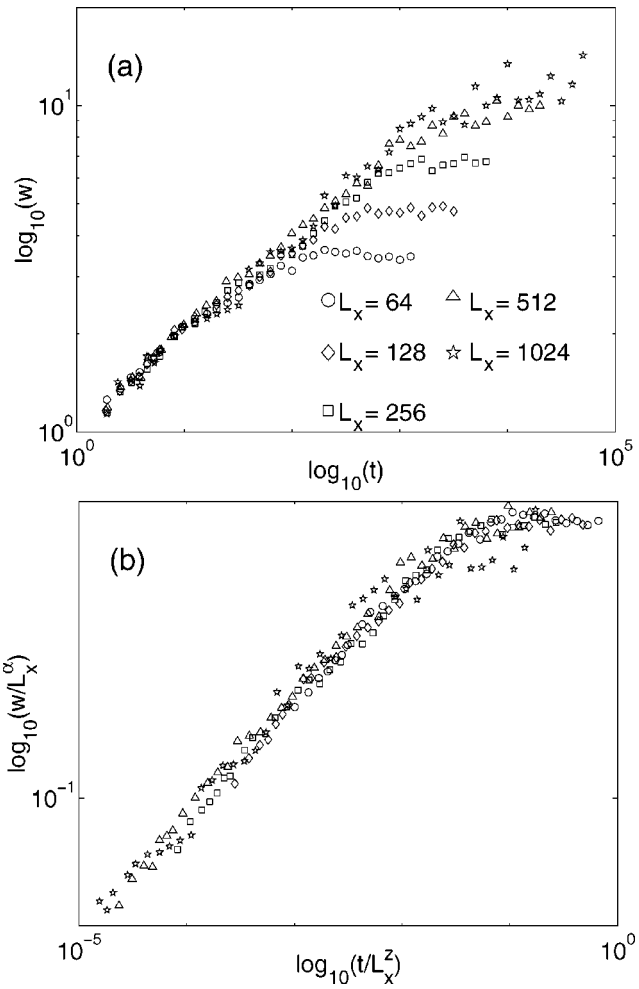

FIG. 4. Scaling of width with the size (a) unscaled and (b) scaled with $\alpha=0.49$, $z=1.81$ from which $\beta=\alpha/z=0.27$. Circles ($L_x=64$), diamonds ($L_x=128$), squares ($L_x=256$), triangles ($L_x=512$), and stars ($L_x=1024$). $L_y=256$ for all cases.

As is typical for a front coarsening problem [4], the time and system size dependence of the mean front width w can be described by a scaling function $g(u)$,

$$w(t)=t^{\beta}g\left(\frac{t}{L_x^z}\right). \tag{8}$$

Here $g(u)$ is constant for $u\ll 1$ and $g(u)\approx u^{-\beta}$ for $u\gg 1$. For $t\gg L_x^z$, the width saturates at $w\sim L_x^{\alpha}$ where $\alpha=\beta z$ is the roughness exponent. Barabási and Stanley [4] have summarized the values of the scaling exponents z, α, and β that are obtained for several experimental systems as well as relevant theoretical results.

In Fig. 4(a) we show w versus t for different system sizes. These data show two characteristic regimes: power law growth, followed by saturation. The growth exponent β is calculated by measuring the slopes of straight line fits to the data before saturation, and the roughness exponent α is cal-

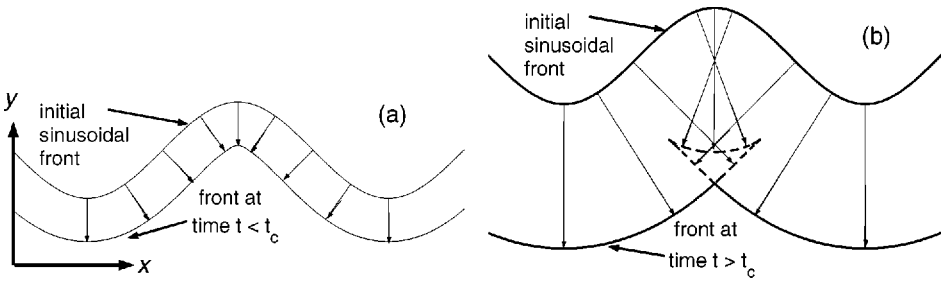

FIG. 5. Geometrical picture of the trajectories given by Eqs. (10) and (11) (a) for $t<t_c$ and (b) for $t>t_c$.

culated by comparing the saturation widths. Figure 4(b) shows w/L_x^{α} versus t/L_x^z, where α and z have been adjusted to $\alpha=0.49$ and $z=1.81$ (corresponding to $\beta=\alpha/z=0.27$). Consistent with Eq. (8), we find the collapse of the data in Fig. 4(a) to a single scaling function. The exponent values we obtain are roughly consistent with those of both the two-dimensional Eden model ($\alpha\cong0.5,\beta\cong0.3$) and the two-dimensional Kardar-Parisi-Zhang equation ($\alpha=1/2,\beta=1/3$) [4,6].

IV. EVOLUTION OF A NON-FLAT FRONT

We now consider the evolution of a front on large length scale. Specifically, we are interested in the case where the front is initially not flat; that is, the position of the front is initially given by $y_0=h(x_0)$. Furthermore, we assume that, as the front evolves, the scale on which the front position varies, $l\approx(h/h')$, remains large compared to the front width,

$$l\gg w. \tag{9}$$

To analyze this situation, we consider that a point on the front moves with a normal velocity $\vec{v}$ whose magnitude, $|\vec{v}|=v$, is constant in time. This assumption also implies that the direction of $\vec{v}$ following the trajectory of a point on the front is constant in time. This is because the slope of the front, dx/dy, following a trajectory does not change with time; i.e., it depends only on the initial location x_0 on the front and not on t. This is illustrated by the construction in Fig. 5(a). As shown in the figure, the trajectory line segments are straight, are all of the same length vt, and are normal to both the initial front and to the evolved front. Considering an initial front position given by $y_0=h(x_0)$, propagation at a velocity $\vec{v}$ normal to the front then yields

$$x(t)=x_0-(vt)h'(x_0)[1+(h'(x_0))^2]^{-1/2}, \tag{10}$$

$$y(t)=h(x_0)-vt[1+(h'(x_0))^2]^{-1/2}. \tag{11}$$

At any given time Eqs. (10) and (11) specify the front position parametrically with x_0 as a parameter. As an example consider the case of an initial sinusoidal undulation of the front $y_0=h(x_0)=C\cos(kx_0)$. As the front propagates, the initial sinusoidal curve becomes distorted so that the maxima become sharp and the minima become broad. As can be seen from Fig. 5(a) this arises because of the converging (diverging) of trajectories that originate near maxima (minima).

Past a critical time $t=t_c$ a cusp develops at the maxima of the evolved front [7]. The cusp formation time is determined by noting that dx/dx_0 first becomes zero at $t=t_c$. From Eq. (10) we obtain

$$t_c=\frac{1}{k^2Cv}. \tag{12}$$

For $t>t_c$ there are pairs of values of x_0 for which the trajectories given by Eqs. (10) and (11) pass through each other. For a given time t greater than t_c we refer to the range of x_0 for which this occurs as the unphysical range. The development of the unphysical range is illustrated in Fig. 5(b) where the dashed portion of the curve shows the result of plotting Eqs. (10) and (11) for the unphysical range.

Figure 6 shows how cusps develop in time. In Fig. 6 the noisy front curves are from our simulations and the smooth curves are from Eqs. (10) and (11) with x_0 restricted to the physical range. The two cases shown in Fig. 6 (namely, $L_x=L_y=128$ and $L_x=L_y=1024$) illustrate how front roughening becomes of less influence as Eq. (9) becomes better satisfied. For both cases in Fig. 6 the initial sinusoid has amplitude $kC=1$ and wave number $k=4\pi/L_x$. Thus from Eq. (12) we have $t_c\sim1/k\sim L_x$. At times $t\sim t_c$, the roughening is a small effect if $kw(t_c)$ is small. Since $w\sim t^{\beta}$ (assuming $t/L_x^z\lesssim1$), we see that $kw(t_c)\sim1/L_x^{1-\beta}$, and roughening will be inconsequential for the large scale front evolution if L_x is sufficiently large. The good agreement of the $L_x=1024$ numerical results from our CCM model with the theory, Eqs. (10) and (11), confirms that the front does indeed propagate at constant velocity in a direction perpendicular to the interface. In particular, for long length scales $l\gg w$ examined in Fig. 6 we see no evidence for curvature dependence of the front velocity.

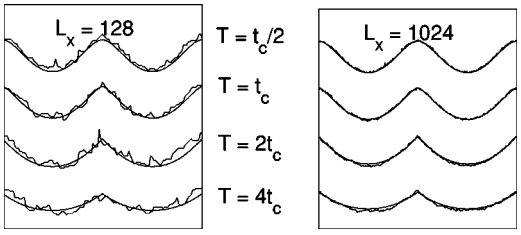

FIG. 6. Comparison between theoretical curves and our 2D simulations for two different system sizes. The front curve from our model is defined as the smallest y value (for given x) at which $\xi=u$, where $u=0.4824$ is the basin boundary point depicted in Fig. 1.

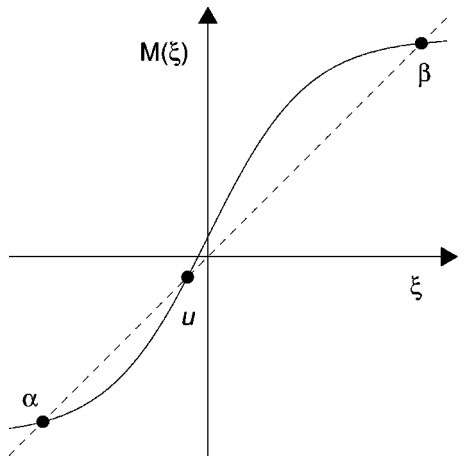

FIG. 7. The map Eq. (13).

As a comparison, we have also considered the propagation of a front between two steady homogeneous states. In particular, replacing $M(\xi)$ in Eq. (3) by

$$M(\xi)=0.1+\tanh(2\xi), \tag{13}$$

we see (Fig. 7) that there are two stable fixed points, α and β, and one unstable fixed point u. Using Eqs. (13), (2), and (5) with a sinusoidal front with initialization of β above the front and at α below the front, we find that the front shape evolves smoothly (with no roughening) according to Eqs. (10) and (11). Thus the cases of a chaotic invading region and a nonchaotic invading region become similar for large L_x (e.g., $L_x \gg w \gg 1/k_0$).

In conclusion, we have introduced a continuum coupled map model for the study of the dynamics of a front separating a region of spatiotemporal chaos from a stable steady region. This model is applicable to periodically forced systems. We find that the front roughens and that this coarsening obeys a scaling hypothesis, Eq. (8). We also investigate the large length scale evolution of a nonplanar front. We find that this evolution is consistent with the hypothesis that, on large scale, the front velocity is constant and normal to the front. This hypothesis and our numerical simulations indicate the formation of cusp structures in the front.

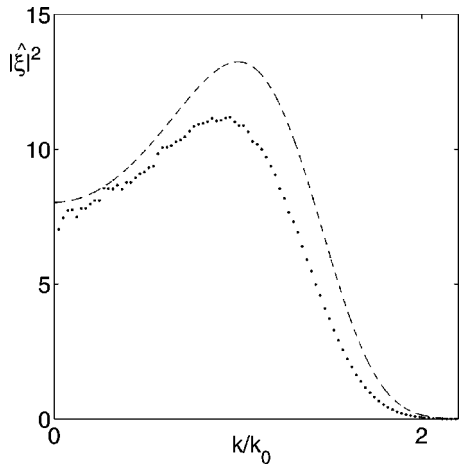

FIG. 8. $|\hat{\xi}|^2$ versus k compared with Eq. (A1).

ACKNOWLEDGMENTS

This work was supported by ONR (Physics). The work of S.C.V. was supported by the Alfred P. Sloan, Jr. Foundation and by the NSF (Grant No. DMR9975533).

APPENDIX

We now comment on the specific form that we have found for $|\hat{\xi}|^2$ [Fig. 2(b)]. In this connection we note that in the limit of a wildly varying map $M(\xi)$ with the Lyapunov exponent approaching infinity $\xi_n'(\vec{x})$ will be wildly varying in space. This is because small variations of $\xi_n(\vec{x})$ with $\vec{x}$ are greatly amplified when M is applied. Thus, in this limit, the spatial correlation function for $\xi_n'(\vec{x})$ will be a δ function, and $|\hat{\xi}_n'(k)|^2=\langle(\xi_n'(\vec{x}))^2\rangle$ independent of $\vec{k}$. Thus from Eq. (2)

$$|\hat{\xi}(k)|^2=\langle(\xi_n'(\vec{x}))^2\rangle f^2(k), \tag{A1}$$

which is plotted in Fig. 8 as the dashed line along with the data from Fig. 2(b). It is seen that Eq. (A1) provides a crude indication of the general form of $|\hat{\xi}(k)|^2$.

[1] W. Losert, D.G.W. Cooper, and J.P. Gollub, Phys. Rev. E **59**, 5855 (1999).

[2] I.V. Melnikov, D.A. Egolf, S. Jeanjean, B.B. Plapp, and E. Bodenschatz, in *Stochastic Dynamics and Pattern Formation in Biological and Complex Systems*, edited by S. Kim, K. J. Lee, T. K. Lim, and W. Sung, AIP Conf. Proc. 501 (AIP, Woodbury, NY, 2000), p. 36.

[3] S.C. Venkataramani and E. Ott, Phys. Rev. Lett. **80**, 3495 (1998).

[4] A.-L. Barabási and H. E. Stanley, *Fractal Concepts in Surface Growth* (Cambridge University Press, Cambridge, 1995).

[5] This general viewpoint was also adopted in Ref. [3] where, motivated by experimentally observed phenomena [F. Melo, P.B. Umbanhowar, and H.L. Swinney, Phys. Rev. Lett. **75**, 3838 (1995)], other choices for M and f were employed. In that case the objective was to check the hypothesis that period doubling in conjunction with pattern formation at a preferred scale were the essential ingredients necessary to explain the observed bifurcations and the evolution of time periodic patterns occurring in a vertically oscillated granular layer of the order of 10 grains thick.

[6] M. Kardar, G. Parisi, and Y.C. Zhang, Phys. Rev. Lett. **56**, 889 (1986).

[7] Cusp formation also occurs for the Kardar-Parisi-Zhang equation; see Fig. 1 of Ref. [6].